Mechanisms and Kinetic Modeling of Calcium Oxalate Crystal Aggregation in a Urinelike Liquor

Part I: Mechanisms

The tendency for aggregation and disruption of aggregates of calcium oxalate dihydrate (CaOx) crystals in urinelike mother liquor was quantitatively studied in a two-stage mixed-suspension, mixed-product-removal crystallizer/Couette-flow aggregator operated in series. The degree of aggregation was obtained by comparing measured number-size and volume-size crystal distributions in the crystallizer and aggregator outlets. Aggregation was a strong function of CaOx supersaturation and may have changed slightly with rotation speed in the Couette-flow aggregator. Rupture of the aggregates increased as the spindle rotation in the aggregator increased (presumably increasing turbulence). Average shear rates in these experiments were appreciably above estimated physiological levels.

R. W. Hartel, B. E. Gottung, A. D. Randolph
Department of Chemical Engineering
University of Arizona
Tucson, AZ 85721

G. W. Drach
Department of Surgery
Arizona Health Sciences Center

SCOPE

Calcium oxalate is one of the main mineral constituents found in kidney stones from patients in developed countries with a high gross national product, presumably because of protein-rich diets. CaOx kidney stone formation in the United States represents a significant medical problem. Such CaOx stones examined *ex vivo* are often found to be polycrystalline aggregates of CaOx crystals. It is likely that aggregation mechanisms play a role in the genesis and retention of such stones. The purpose of this study was to quantitatively examine the formation of aggregates in a urinelike liquor to specifically study the effects of average shear rate (aggregator rotation rate) and CaOx supersaturation.

CONCLUSIONS AND SIGNIFICANCE

The degree of aggregation in the experimental apparatus could be quantitatively expressed by several statistical measures, e.g., the decrease in crystal numbers through the aggregator (normalized by total number in the crystallizer), the increase in crystal numbers above 15 μm, and the increase in average particle volume. All three of these statistical measures of aggregation correlated strongly with aggregator rpm and $[Ox^{2-}]$ feed concentration. Maxima in aggregation vs. rotator speed curves coincided with the predicted onset of Taylor turbulence instabilities within the flow pattern. Increased shear rate up to the point of turbulence increased aggregation. Aggregation increased with increasing $[Ox^{2-}]$, indicating the formation of more stable particle clusters at higher supersaturations.

These data should be useful to the urologist in constructing theoretical models of kidney stone formation. The experimental technique and data analysis should prove useful in the study of aggregation phenomena in other systems.

Introduction

An *ex vivo* calcium oxalate stone is often observed to be composed of many individual crystallites firmly cemented together as one mass. Such polycrystalline conglomerates are properly designated as aggregates[1] and aggregation mechanisms are quite likely involved in the overall mechanism of stone formation. [Definitions consistent with current ASTM usage are adopted in this study to differentiate flocculates, aggregates, and agglomerates (ASTM, 1985). These definitions are at variance with some previously used definitions of agglomerates, e.g., Irani and Callis (1963). Thus a flocculate is a group of two or more particles held together by weak cohesive forces, whereas an agglomerate consists of a tightly bound mass formed by the cementation of individual particles, probably by chemical forces. ASTM (1985) differs from ASTM (1984), but is consistent with general European usage. ASTM (1985) defines aggregates as clusters of particles having a binding force intermediate between agglomerates and flocculates. Within the spirit of ASTM (1985) we use the single term aggregates to describe the weakly-cemented crystal clusters of this study, unless otherwise stated in the text.]

There are many unresolved questions as to the role of aggregation in the formation of a stone, e.g., "Does aggregation occur in a two-step process, with flocculation followed by tight crystal-crystal bonding into aggregates? What is the quantitative role of supersaturation in the overall aggregation mechanism? Do high molecular weight macromolecules that naturally occur in human urine aid or hinder aggregation?" These and other questions can be answered using the two-stage continuous-flow aggregator that was developed for this study.

The incidence of kidney stones can be related to many factors. While an individual's stress level and dietary habits are primary causes (Robertson et al., 1980; Brundig, et al., 1981), the occurrence of kidney stones has also been correlated with heredity, race, age, sex, climate, and occupation (Blomen, 1982; Robertson et al., 1974). In people who exhibit a propensity to form kidney stones, these factors can generally be related to increased concentrations of mineral salts in the urine (Finlayson, 1978), specifically calcium and oxalate. This results in higher supersaturations in the urine and increased stone production. While calcium oxalate (CaOx) is the major constituent of kidney stones, other mineral salts are also frequently found in stones. These include calcium phosphate, magnesium ammonium phosphate, magnesium phosphate, diammonium urate, and calcium acid urate. Typically, more than 97% of a kidney stone is a polycrystalline aggregate of mineral salts, with the remaining 3% consisting of a protein and carbohydrate substance called matrix (Boyce and Garvey, 1956). It is not yet clear how these constituents combine to form kidney stones.

For kidney stones to form, several events must occur. First, the ionic concentrations of the mineral salts in the kidney must exceed the critical concentration for nucleation to occur. This may occur as homogeneous nucleation (Resnick and Boyce, 1979) or as heterogeneous nucleation on a foreign impurity. The stone nuclei must then grow to a large enough size to remain in the kidney. Finlayson (1978) has shown that this cannot be ascribed solely to molecular growth, due to the short residence time of urine in the kidney. Aggregation of the small CaOx nuclei most likely accounts for the growth of stones encountered in the kidney. Parameters that affect the aggregation rate are the surface electrical potential of the salt nuclei and the collision frequency of these nuclei, which is determined by the flow field in the kidney. Once flocculates are formed, they apparently can bridge together to form bonded aggregates, provided that the surrounding liquid remains supersaturated. An aggregate can then grow, by further aggregation, to a size at which it can get trapped in the kidney. Alternatively, a stone may form initially by nucleation of the mineral salts directly onto a membrane surface. It can then grow by a combination of molecular growth and aggregation.

The actual mechanistic steps resulting in aggregation of the CaOx nuclei into kidney stones are not clearly understood. The nuclei must first be brought near to each other through some collision mechanism. This may be induced by Brownian motion, laminar shear flow, or turbulent flow. A combination of these mechanisms probably occurs in the kidney, with collision by Brownian motion dominating for nuclei less than about 1 μm size and laminar shear and/or turbulent flow collisions causing aggregation of larger crystals. Once the nuclei are brought into contact by collision, surface properties determine whether they stay together. Adair (1981) has shown that calcium oxalate monohydrate follows classical coagulation theory based on the electrical double layer surrounding the particles. As the surfaces of any two particles would assume the same electrical potential, regardless of size, then these forces due to surface potential are always repulsive and act to counter the attractive body forces (Van der Waals). An increase in ionic strength of the surrounding fluid can act to "compress" the repulsive force field surrounding the particles and thus increase the flocculation rate.

The macromolecular protein polymers existing in human urine might effect the aggregation rate in two different ways. First, they might adsorb to the crystal surfaces and form a bridge between the two colliding nuclei (Finlayson, 1978). Alternatively, the adsorbed polymers might reduce the flocculation rate by altering the electrical double layer. Drach et al. (1984) have shown that, in fact, aggregation is reduced by nearly a factor of two when these macromolecular proteins are present. The overall aggregation rate of CaOx nuclei might be influenced by any one of these individual mechanisms.

The extent of aggregation in batch systems has been related to the differences between the initial crystal size distribution and the distribution at some later point in time. In a continuous system, the initial distribution is fed into the aggregator and compared to the product distribution. The parameters most commonly employed (Sastry and Fuerstenau, 1970; Halfon and Kaliaguine, 1976; Swift and Friedlander, 1964; Suzuki, 1981) to characterize the changes in crystal size distribution (CSD) are the total number of crystals, N_T, the number of large crystals greater than some arbitrary size L_o, and the mass-weighted average size, $\bar{L}_{4,3}$. Changes in these parameters were used in the present study to quantify the extent of aggregation. When aggregation occurs it would be expected that the total number of crystals would decrease, the number of large crystals would increase, and the mass-weighted average size would increase.

The purpose of this study was to quantify the aggregation of CaOx crystals as a separate phenomenon from their nucleation and growth in order to better understand kidney stone formation. Crystals of CaOx were nucleated from a synthetic urine solution in an intensely stirred mixed-suspension, mixed-product-removal (MSMPR) crystallizer and then aggregated in a Couette-flow aggregator. Crystal size distributions were ob-

tained from each vessel using an in-line measuring device. The extent of aggregation was quantified by the change in total number between the crystallizer and aggregator, $\Delta N_{T(C-A)}/N_{T(C)}$, the change in number of large (>15 μm) crystals, $\Delta N^{15}_{(A-C)}/N_{T(C)}$, and the change in the mass-weighted average size, $\Delta L_{4,3(A-C)}/N_{T(C)}$. These parameters were normalized by the total number of crystals exiting the crystallizer to account for variations between experiments in the number of crystals entering the aggregator. Changes in aggregation were related to changes in the rpm of the aggregator spindle and to increases in the supersaturation level. The main advantages in this study of using a continuous system are:

- A reproducible distribution of fresh seed crystals can be generated in their own mother liquor, as in the kidney.
- The number-size distribution of the seed crystals can be quantitatively extrapolated below measurement size using the exponential form of the MSMPR distribution, thus facilitating kinetic modeling, which is presented in Part II of this study.

Experimental

A flow diagram of the experimental apparatus is shown in Figure 1. Calcium oxalate dihydrate crystals were precipitated in a synthetic urine solution (Gottung, 1983) in a MSMPR crystallizer similar to that described by Thorson (1979) and Kraljevich (1981). The MSMPR crystallizer was maintained at 37°C and had a residence time of 10 min. The annular volume in the aggregator was essentially equal to the crystallizer volume, thus giving an overall residence time through the system of about 20 min. The initial concentrations, based on total feed volume, were 6.0 mM calcium and 0.6 mM oxalate. This 10:1 Ca/Ox ratio approximates the ratio of these ions in typical human urine. The CSD of the crystallizer closely approximated the expected exponential MSMPR distribution.

The product of the crystallizer was passed through a Couette-flow aggregator. This aggregator consisted of two concentric cylinders with the inner cylinder rotating. The inside diameter of the outer cylinder was about 69.4 mm and the outer diameter of the rotating cylinder was about 51 mm, thus giving an annular space of approximately 9.2 mm. Thus at a typical spindle rotation speed of 80 rpm the average shear rate in the annulus would be about 23 s^{-1}. These levels are above the physiological rates of 3 to 5 s^{-1} estimated in small urinary tubules (Adair, 1981). The CSD of both the aggregator and crystallizer was measured in-line using a PDI Electrozone/Celloscope particle counter equipped with a 150 μm orifice tube. The changes due to aggregation were quantified by comparison of the two distributions.

Two parameters that affected the degree of aggregation were the rpm of the inner cylinder and the concentration of oxalate in the aggregator. The rotational velocity of the inner cylinder was varied between 80 and 250 rpm, which changed the flow patterns in the annulus. The oxalate concentration was varied by addition of a low-volume stream of oxalate solution directly into the aggregator. The range of oxalate concentrations was from 0.6 mM (with no oxalate addition) to 1.8 mM. These concentrations are expressed as equivalent oxalate concentration in the crystallizer feed, as though all oxalate were added at this point. Oxalate concentrations in the crystallizer and aggregator are, of course, dependent variables and cannot be set independently. The level of oxalate was expressed as an equivalent feed concentration for simplicity because no reliable oxalate analysis in urinelike liquors was available to the authors.

Further details of the experimental apparatus and procedure are available in Gottung (1983).

Results

One indication of aggregation is the increase in the mass-weighted average size of the initial distribution. Figure 2 shows this increase for a typical run and clearly illustrates the shift of the whole distribution toward the larger sizes. This shift can be attributed to aggregation rather than growth since the total number of crystals was found to decrease in the aggregator compared to the crystallizer. A plot of the population density function vs. the crystal size, as shown in Figure 3 for 80 rpm, also clearly shows aggregation. There are fewer small particles and more large particles in the aggregator distribution. This shows a classic aggregation pattern as the small particles stick together to form large particles. This shift in the distribution was found

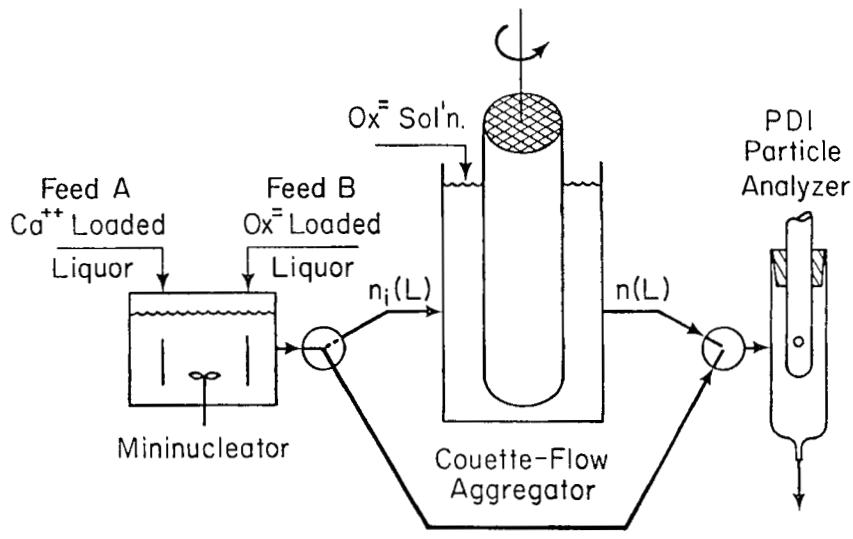

Figure 1. Diagram of mininucleator/aggregator apparatus.

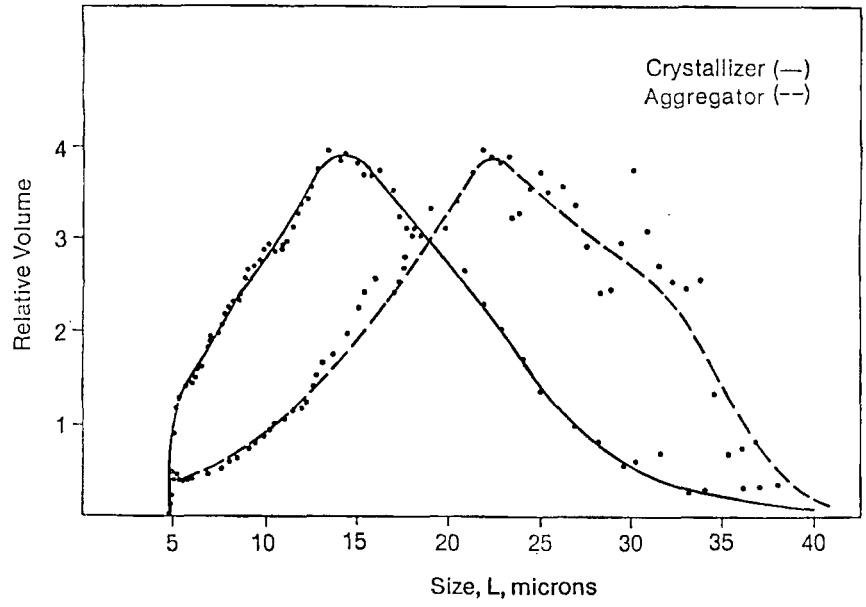

Figure 2. Comparison of typical volume distribution from crystallizer and aggregator.

to change as the inner cylinder rpm and the aggregator supersaturation level changed. It is recognized that the shear flow field set up is not physiological; variable shear rates were used in this study to promote aggregation at different rates and to study the tightness of bonding of the aggregated particles.

RPM

The control experiment performed at 0 rpm showed that no aggregation occurred in the absence of a shear field. In fact, it was found that the only changes in the distribution could be attributed to the settling out of larger crystals due to the lack of agitation in the apparatus.

The aggregation parameters, $\Delta N_{T(C-A)}/N_{T(C)}$, $\Delta \bar{L}_{4,3(A-C)}/N_{T(C)}$, and $\Delta N_{(A-C)}/N_{T(C)}$, were found to vary as the rpm of the inner cylinder was changed. Variations in these parameters are shown in Figures 4–6.

The change in total number of crystals between crystallizer and aggregator is shown in Figure 4. As the rpm increased to approximately 120, the number of crystals in the aggregator decreased, thus causing $\Delta N_{T(C-A)}$ to increase. Above 120 rpm the difference between total crystal number, crystallizer minus agglomerator, was less pronounced. At all values of rpm, the total number in the aggregator was less than the total number in the crystallizer, indicating that some aggregation took place.

The mass-weighted average size, $\Delta \bar{L}_{4,3(A-C)}/N_{T(C)}$, changed in a similar manner, as seen in Figure 5. The average size in the aggregator increased as the speed increased up to approximately 150 rpm. Above this speed, the average size decreased from its maximum.

Figure 6 shows how the change in the number of larger crystals (>15 μm) varied with rpm. The number of crystals larger than 15 μm was always greater in the aggregator distribution and the difference between aggregator and crystallizer increased steadily as the rpm increased.

The normalized population densities, $N_{(A)}(L)/N_{T(A)}$, for the aggregator distributions at the various rpm values are shown in Figure 7, showing how the actual distributions varied with the rpm. In general, the number of smaller crystals (5–9 μm) decreased steadily with rpm. At the same time, the number of crystals between 10 and 18 μm increased significantly as the rpm increased above 150 rpm. The number of the largest crystals increased with rpm at low rpm values, but then began to decrease as the rpm increased above 150 rpm. These changes caused a hump in the distribution between 10 and 18 μm at the higher values of rpm.

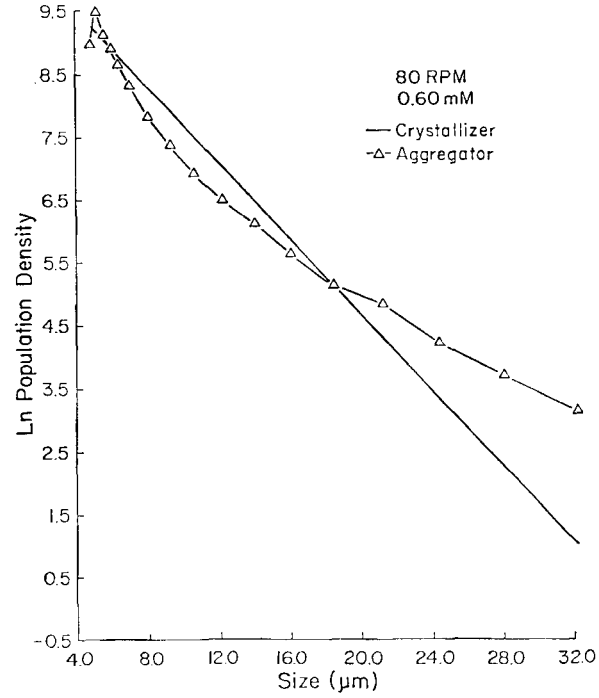

Figure 3. Comparison of typical population density distributions from crystallizer and aggregator.
Data for experiment 3/17 with population density expressed in size coordinates (no./mL · μm).

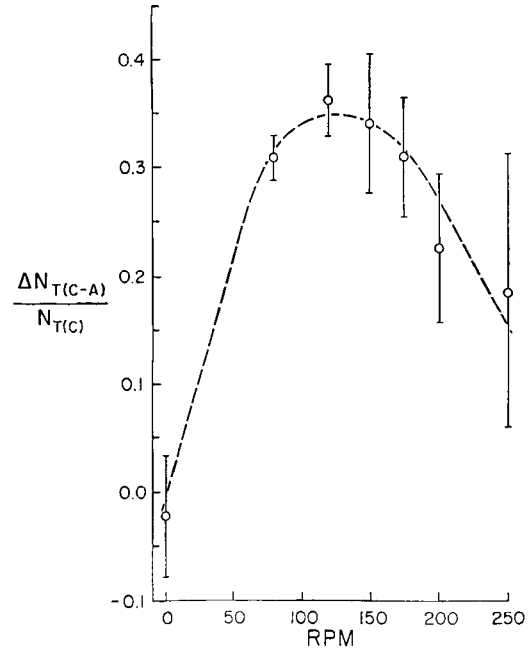

Figure 4. Change in total number of crystals between crystallizer and aggregator, $\Delta N_{T(C-A)}/N_{T(C)}$, vs. inner cylinder rpm of aggregator.

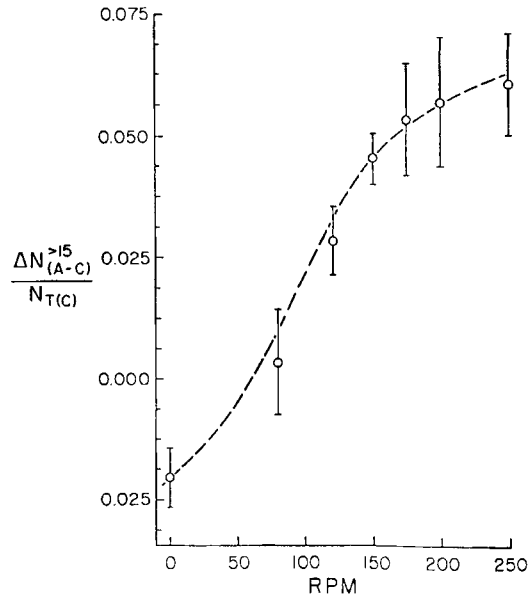

Figure 6. Change in number of crystals greater than 15 μm between aggregator and crystallizer, $\Delta N^{>15}_{(A-C)}/N_{T(C)}$, vs. inner cylinder rpm of aggregator.

Concentration

Figures 8–10 show how the aggregator parameters varied as the oxalate concentration in the aggregator changed while the rpm was maintained at 150. Although oxalate was added directly to the aggregator, the concentration is expressed as if an equivalent amount of oxalate were added to the crystallizer in the initial feed concentration. Oxalate was reported in this fashion due to the lack of a simple and accurate oxalate assay in urinelike solutions.

Figure 8 shows that the change in total number of crystals between the crystallizer and aggregator, $\Delta N_{T(C-A)}/N_{T(C)}$, increased as the oxalate concentration increased. Hence, the total number of crystals in the aggregator decreased with increasing oxalate concentration.

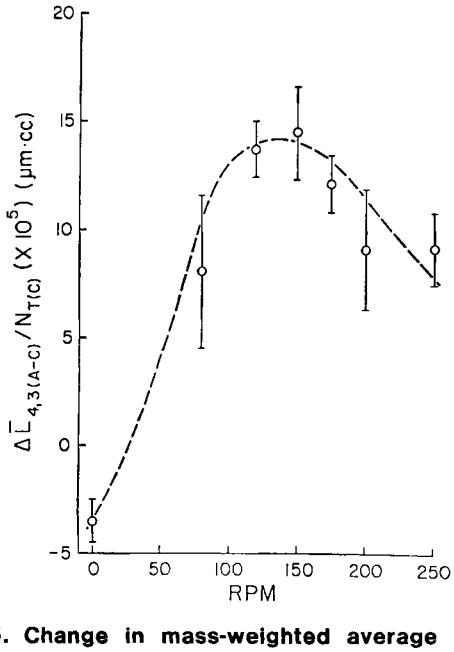

Figure 5. Change in mass-weighted average size between aggregator and crystallizer, $\Delta \bar{L}_{4,3(A-C)}/N_{T(C)}$, vs. inner cylinder rpm of aggregator.

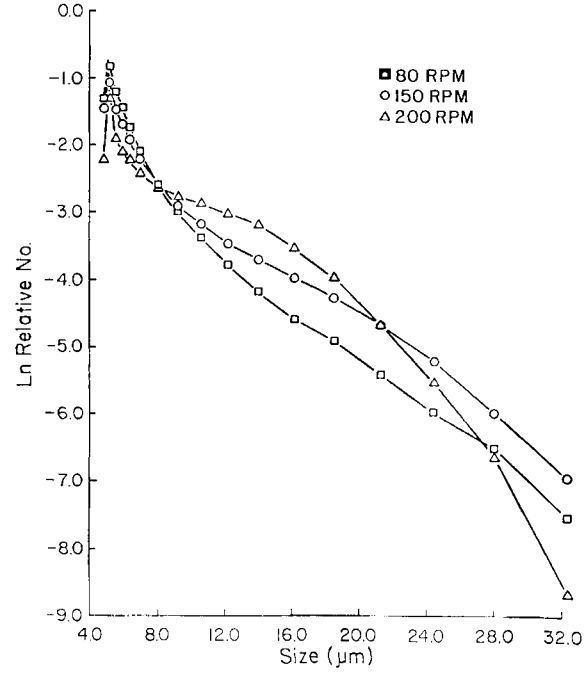

Figure 7. Effect of inner cylinder rpm on average relative number, $N_{(A)}/N_{T(A)}$, in the aggregator.

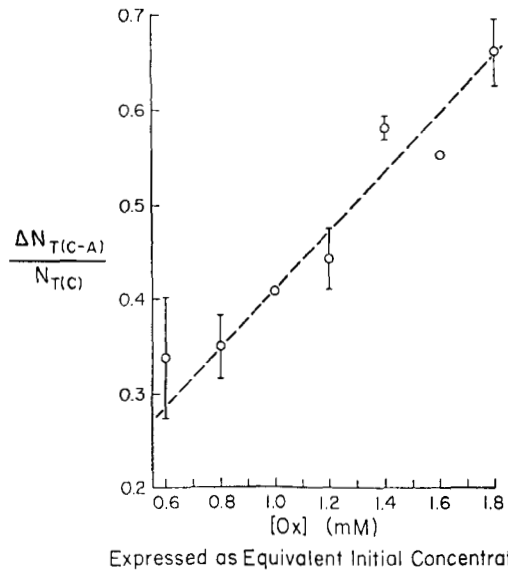

Figure 8. Change in total number of crystals between crystallizer and aggregator, $\Delta N_{T(C-A)}/N_{T(C)}$, vs. oxalate concentration in the aggregator.

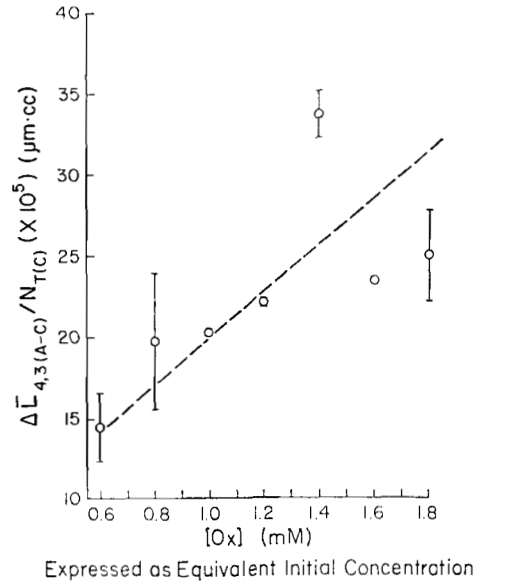

Figure 10. Change in mass-weighted average size between aggregator and crystallizer, $\Delta \bar{L}_{4,3(A-C)}/N_{T(C)}$, vs. oxalate concentration in the aggregator.

The number of larger crystals, greater than 15 μm also decreased as the oxalate concentration increased, as shown in Figure 9. This is an apparent anomaly that might have been due to settling out or wall fouling by some of the large aggregates. The mass-weighted average size, however, increased with oxalate concentration. This effect is shown in Figure 10. These results must be interpreted with some caution, however, as it was qualitatively observed that more large particles settled out, and consequently were not counted, at the higher concentrations. No measurement of the mass lost due to settling out was made. The relative change in the aggregator distributions at various oxalate concentrations is shown in Figure 11. In general, the number of particles at all sizes decreased as the oxalate concentration increased.

Several experiments were performed at 200 rpm and equivalent oxalate concentrations of 1.0 and 1.8 mM to determine the changes in disruption of aggregates. The results were qualita-

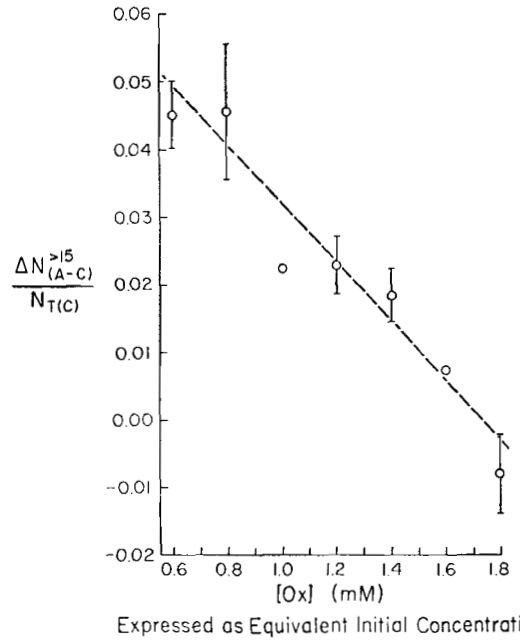

Figure 9. Change in number of crystals greater than 15 μm between aggregator and crystallizer, $\Delta N^{>15}_{(A-C)}/N_{T(C)}$, vs. oxalate concentration in the aggregator.

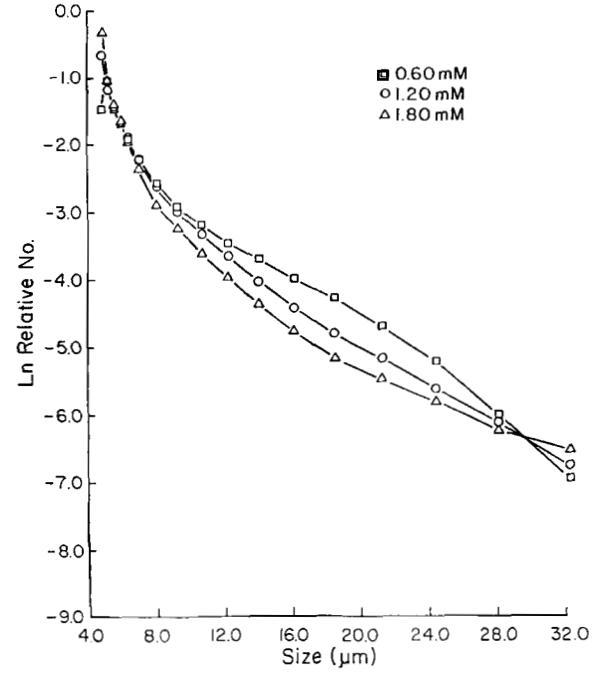

Figure 11. Effect of oxalate concentration in the aggregator on average relative number, $N_{(A)}(L)/N_{T(A)}$, in the aggregator.

tively the same as obtained for increased oxalate concentration experiments at 150 rpm. The degree of disruption decreased as the oxalate concentration increased, with slightly higher levels of disruption than at 150 rpm.

Total volume changes

The experimentally determined aggregator and crystallizer distributions were integrated numerically from 5 to 30 μm to determine changes in total volume. These changes were then correlated with the changes in rpm and oxalate concentration.

The change in total volume of crystals between the aggregator and crystallizer was expressed as $\Delta V_{T(A-C)}/V_{T(C)}$. This parameter is equivalent to the normalized change in total mass of crystals occurring in the aggregator. Figures 12 and 13 show the changes in total mass as the rpm and oxalate concentration were varied.

Figure 12 indicates that the total mass of the aggregator distribution increased as the rpm was increased. However, as the oxalate concentration increased, the total mass of the aggregator distribution decreased, as seen in Figure 13.

Analysis and Discussion

Couette-flow aggregator

The effect of changing rpm on the flow field in the aggregator must be understood before the aggregation data can be fully explained. This type of annular flow has been studied in great detail, most notably by Couette (1890) and Taylor (1923). It was found that the pure shear flow that existed for very low cylinder velocities became unstable as the rpm increased beyond a certain point. This critical point was found to depend also on the geometry of the apparatus and on the fluid system being studied. The flow field can then be related to a dimensionless number, attributed to Taylor and given by the following expression:

$$Ta = \frac{2\pi}{60}\frac{R_i^{1/2}\,d^{3/2}}{\upsilon}N \qquad (1)$$

Instabilities appear initially as pairs of counterrotating vortices as shown in Figure 14. These vortices change their characteristics as the Taylor number is increased. Kataoka et al. (1975) separated the flow patterns into five distinct flow regimes, as given in Table 1. When Ta is approximately Ta_{cr}, the vortices remain quite distinct. However, as Ta increases they

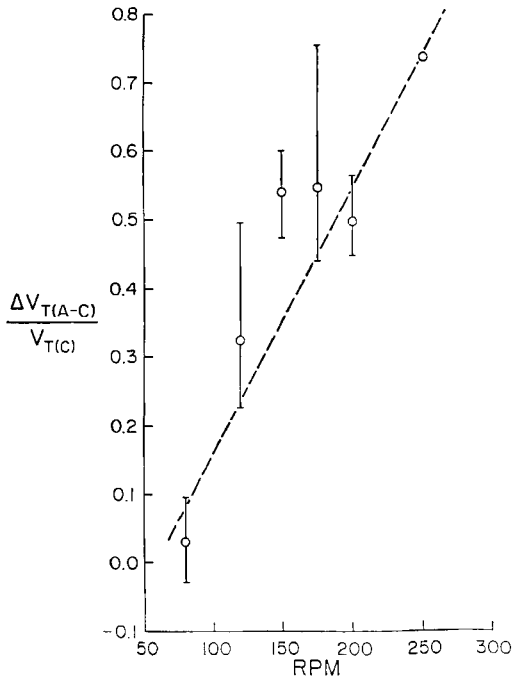

Figure 12. Change in total volume of crystals between aggregator and crystallizer, $\Delta V_{T(A-C)}/V_{T(C)}$, vs. inner cylinder rpm.

$V_T = \int_{L-5}^{L-30} \upsilon n(\upsilon)\, d\upsilon$.

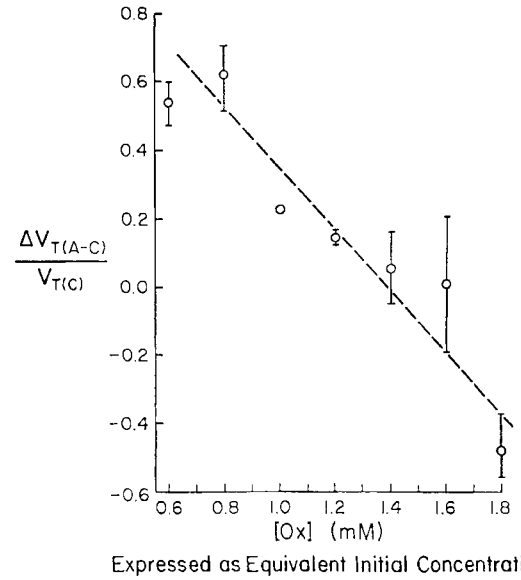

Figure 13. Change in total volume of crystals between aggregator and crystallizer, $\Delta V_{T(A-C)}/V_{T(C)}$, vs. oxalate concentration in the aggregator.

$V_T = \int_{L-5}^{L-30} \upsilon n(\upsilon)\, d\upsilon$.

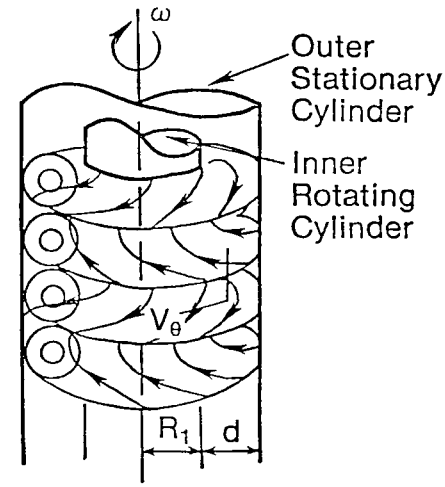

Figure 14. Diagram of Couette-flow apparatus with axial distribution of Taylor vortices (after Kataoka et al., 1975).

Table 1. Flow Regimes for Rotational Couette Flow*

1. Laminar Flow ($Ta < Ta_{cr}$)
   - Pure shear flow
   - Ta_{cr} is point where flow becomes unstable
2. Laminar Vortex Flow (singly periodic) ($Ta_{cr} < Ta < 800$)
   - Taylor vortices appear as stacks of toroids
   - Pairs of vortices rotating in opposite directions resulting in inflow boundaries and outflow boundaries
   - As Ta increases toward 800, oscillations in vortex boundaries occur, appearing as axial traveling waves
3. Transition Flow (doubly periodic) ($800 < Ta < 2{,}000$)
   - Oscillations in vortex boundaries occur in increasingly complex patterns as the vortices become increasingly unstable
4. Turbulent Vortex Flow ($2{,}000 < Ta < 10$–$15{,}000$)
   - Turbulent eddies visible within vortex structure
   - Vortices beginning to break up
5. Turbulent Flow ($Ta > 15{,}000$)
   - Turbulent eddies dominate
   - Some vortex structure still remains

*Kataoka et al. (1975).

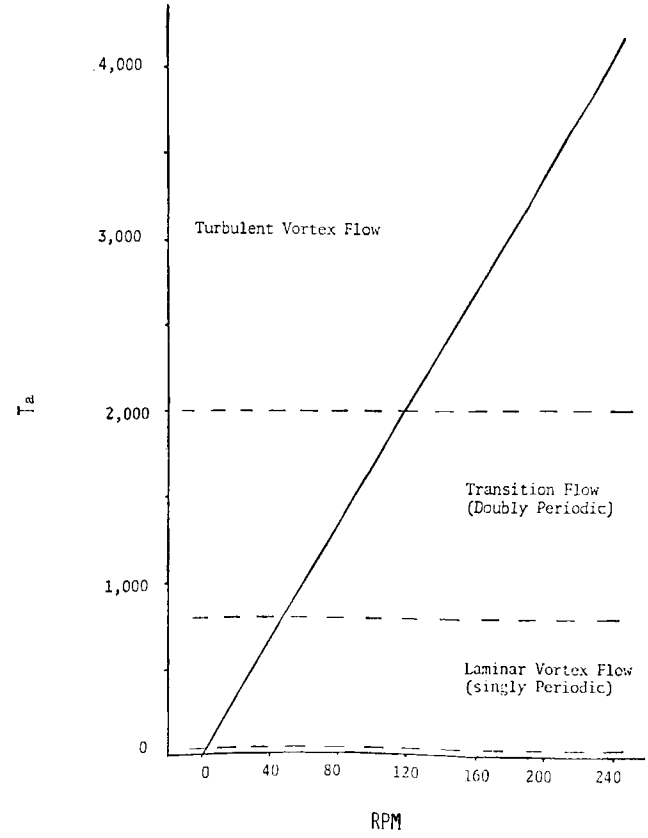

Figure 15. Flow regimes for Couette-flow aggregator where the Taylor number is defined by Eq. 1.

become increasingly unstable. In the laminar vortex region, singly periodic traveling waves exist that distort the boundaries of the vortices. These waves become more energetic as Ta approaches 800. Above this value, another oscillation appears that further distorts the vortex structure, with an increasing degree of oscillation in the vortex boundaries caused by several traveling waves. As Ta increases above 2,000, the energy of these oscillations is great enough to cause turbulent breakup within the vortices. Further increases in Ta result in greater dominance of turbulence over the vortex structure until the flow becomes purely turbulent at very high Ta. Excellent photographs of these various flow patterns can be seen in Coles (1965).

For a given system, the Taylor number is a linear function of the inner cylinder velocity. Figure 15 shows how Ta varies with rpm for the laboratory aggregator used in this study. The variation of rpm between 80 and 250 causes a change in flow regimes from the doubly periodic flow to turbulent vortex flow, with the change occurring at about 150 rpm. This shift in flow corresponds quite closely to the point where the aggregation data (Figures 4 and 5) begin to change characteristics. That is, the hump in the distribution, as seen in Figure 7, becomes quite evident at approximately 150 rpm. This suggests a change in the mechanism of aggregation as the rpm is increased.

Mechanisms of Aggregation

It is now possible to suggest a physical process to explain the aggregation of CaOx in the Couette-flow apparatus. At low inner cylinder velocities, the flow is in the doubly periodic regime. The flow patterns are quite energetic and cause a high number of collisions of CaOx nuclei. The nuclei then stick together and appear as larger particles. This classical case of aggregation results in a decrease in the number of small crystals and an increase in the number of large crystals. This pattern was observed at 80 to 120 rpm.

As the rpm increases to 150 and above, turbulent eddies appear within the vortex structure. These turbulent eddies have enough energy to disrupt some of the aggregates, especially the larger ones, causing the number of very large crystals (22–30 μm) to decrease. The decrease in $\Delta\bar{L}_{4,3(A-C)}/N_{T(C)}$ above 150 rpm shown in Figure 5 indicates that disruption increased with rpm. The changes in $\Delta N_{T(C-A)}/N_{T(C)}$ and $\Delta N^{15}_{(A-C)}/N_{T(C)}$ show that even though the number of small crystals decreased slightly, the total number of crystals increased with rpm above 150 due to the increased production of medium-size crystals from the disruption of large crystals. This increased production of medium-size crystals resulted in a continuous increase of the number of crystals greater than 15 μm, as shown in Figure 6.

Increasing aggregation and disruption rates can also explain the variation in the change in total volume between aggregator and crystallizer, as seen in Figure 12. Increased aggregation would bring more mass into the distribution from particles below the 5 μm measurement limit and increased disruption would prevent the loss of mass due to settling out of large (>30 μm) particles. Therefore, the total mass (or volume) in the aggregator distribution should increase with increasing rpm.

This proposed mechanism of combined aggregation and rupture of CaOx crystals suggests that at these conditions, the aggregates are yet weakly bonded and are subject to disruption at the higher rpm's and lower oxalate concentrations. In order for aggregation to occur, the flocculates must be cemented together. This can occur by increased crystal growth between the flocculated crystallites or by increased probability of particles sticking together by altering the surface characteristics. The latter may be caused by changes in electrostatic repulsion and/or compression of the electrical double layer surrounding the crystal. The addition of oxalate ions to the aggregator would

cause all of the above to occur. Thus, an increase in oxalate concentration would decrease the amount of disruption and increase the apparent aggregation rate.

In fact, less disruption and more aggregation was observed as the oxalate concentration in the aggregator was increased. The results shown in Figure 11 indicate quite clearly that the aggregation rate increased as the oxalate concentration increased. The disruption rate of the larger crystals was seen to decrease, as shown by the decreased number of all crystals, although this effect may be masked somewhat by an increased aggregation rate and an increased settling rate of the very large aggregates. These results can also be seen in Figure 13, where the total volume in the aggregator distribution is shown to decrease as the oxalate concentration increases, due to the loss of large particles *out of the* observable size range and increased fouling on the aggregator walls.

Conclusion

An experimental technique that separated the effects of aggregation from nucleation and growth was employed to study the aggregation of calcium oxalate crystals. This technique has general application to the study of aggregation phenomena in other crystal systems.

A MSMPR crystallizer was used to feed a known distribution of CaOx crystals into a Couette-flow aggregator. The resulting change in the crystal size distribution due to the aggregation process was studied as a function of inner cylinder rpm and oxalate concentration in the aggregator. Varying the inner cylinder rpm changed the flow patterns in the aggregator annulus, which in turn changed the collision rate of crystals. Increasing the oxalate concentration increased the supersaturation in the aggregator and served to change the growth rate and binding forces of the colliding crystals. Both parameters had a pronounced effect on the aggregation rate.

Increasing the inner cylinder rpm from 80 to 250 rpm affected the aggregation rate of crystals to a small degree as seen by decreases in the number of smaller crystals (5–12 μm) and increases in the number of larger crystals (15–30 μm). As the rpm was increased above 150, the disruption of large (22–30 μm) crystals also increased, as evidenced by a decrease in the number of these large crystals along with an increase in mid-size crystals (12–20 μm). The majority of the changes in aggregator CSD caused by changing rpm could be explained by changes in disruption rates of aggregates. This increase in disruption rate beginning at approximately 150 rpm correlated well with the onset of turbulence in the flow field of the Couette-flow aggregator.

An increase in oxalate concentration in the aggregator from 0.6 to 1.8 mM (concentrations based on equivalent initial concentration) also resulted in increased aggregation. In this case, the increased physical attraction of the crystals at higher oxalate levels increased the aggregation rate. It was also found that the increased binding forces also decreased the disruption rate of aggregates. This decreased disruption rate indicates that more tightly bound aggregates were formed at higher Ox concentrations.

Solution of the population balance equation with various models of aggregation and disruption would aid in confirming the mechanisms that control the change in size distribution of CaOx crystals in the Couette-flow aggregator. Computer modeling of these data using the general population balance equation is presented in Part II.

Acknowledgment

This work was supported by National Science Foundation Grant No. CPE-8117753. A. D. Randolph wishes to acknowledge partial sabbatical support (1982) from the British SERC (Science and Engineering Research Council) for study of CaOx nucleation and aggregation mechanisms.

Notation

d = annulus width of Couette-flow aggregator, cm
L = crystal size, μm
$\Delta\bar{L}_{4,3(A-C)}$ = change in mass-weighted average size between aggregator and crystallizer, μm
$n(L)$ = population density distribution function, no./mL · μm
N = revolutions per minute
$N_{(A)}(L)$ = number of crystals in aggregator distribution, no./mL
$\Delta N^{>L_o}_{(A-C)}$ = change in number of crystals greater than some size L_o between aggregator and crystallizer, no./mL
$\Delta N_{T(C-A)}$ = change in total number of crystals between crystallizer and aggregator, no./mL
R_i = inner cylinder radius of Couette-flow aggregator, cm
Ta = dimensionless Taylor number
$\Delta V_{T(A-C)}$ = changes in total volume of crystals between 5 and 30 μm between aggregator and crystallizer, mL/mL
υ = kinematic viscosity, cm^2/min

Literature cited

Adair, J. H., "Coagulation of Calcium Oxalate Monohydrate Suspension," Ph.D. Diss., Univ. Florida, Gainesville (1981).

ASTM, *Designation E20-68 (Reapproved 1974), General Methods and Instruments,* **14.02,** 19 (1984).

ASTM, *Designation E20-85, General Methods and Instruments,* **15.02,** 18 (1985).

Blomen, L. J. M., "Growth and Aglomeration of Calcium Oxalate Monohydrate Crystals," Ph.D. Diss., University of Leiden, Netherlands (1982).

Boyce, W. I., and F. K. Garvey, "The Amount and Nature of the Organic Matrix in Urinary Calculi: A Review," *J. Urol.,* **76,** 213 (1956).

Brundig, P., W. Berg, and J. J. Schneider, "Stress and Risk of Urolith Formation in the Influence of Stress on Litholytic Urinary Substances," *Urol. Int.,* **36,** 265 (1981).

Coles, D., "Transition in Circular Couette Flow," *J. Fluid Mech.,* **21**(3), 385 (1965).

Couette, M. M., "Etudes sur le Frottement des Liquides," *Ann. Chem. Phys., 6th ser.* **21,** 433 (1890).

Drach, G. W., et al., "Effects of Human Urine on the Aggregation of Calcium Oxalate Crystals: Normal Persons vs. Stone-formers," *Proc. 5th Int. Conf. Urolithiasis,* Garmish, W. Germany (1984).

Finlayson, B., "Physicochemical Aspects of Urolithiasis," *Kidney Int.,* **13,** 344 (1978).

Gottung, B. E., "Calcium Oxalate Agglomeration in Urinelike Liquors," M.S. Thesis, Univ. Arizona, Tucson (1983).

Halfon, A., and S. Kaliaguine, "Aluminatrihydrate Crystallization. 2: A Model of Agglomeration," *Can. J. Chem. Eng.,* **54,** 168 (1976).

Irani, R. R., and C. F. Callis, *Particle Size: Measurement, Interpretation and Application,* Wiley, New York, pp. 17–18, (1963).

Kataoka, K., et al., "Ideal Plug-Flow Properties of Taylor Vortex Flows," *J. Chem. Eng. Japan,* **8**(6), 472 (1975).

Kraljevich, Z. I., "Effect of Urinary Macromolecules on Crystallization of Calcium Oxalate in Synthetic Urine solutions," Ph.D. Diss., Univ. Arizona, Tucson (1981).

Resnick, M. I., and W. H. Boyce, in *Urinary Calculous Disease,* J.E.A. Wickman, ed., Churchill Livingstone, New York (1979).

Robertson, W. G., et al., "Seasonal Variations in Urinary Excretion of Calcium," *Brit. Med. J.,* **4,** 436 (1974).

———, "Epidemiological Risk Factors in Calcium Stone Disease," *Proc. Symp. on Urolithiasis* (1979), *Scand. J. Urol. Nephrol. Suppl.,* **53,** 15 (1980).

Sastry, K. V. S., and D. W. Fuertstenau, "Size Distribution of Agglomerates in Coalescing Dispersed Phase Systems," *IEC Fund.*, **9**(1), 145 (1970).

Suzuki, K., "Studies on Urolithiasis: Crystal Aggregation in Calcium Oxalate Stone-formers," *Japan Urol. Assoc. J.*, **72**(7), 841 (1981).

Swift, D. L., and S. K. Friedlander, "The Coagulation of Hydrosols by Brownian Motion and Laminar Shear Flow," *J. Colloid Sci.*, **19**, 621 (1964).

Taylor, G. I., "Stability of a Viscous Liquid Contained between Two Rotating Cylinders," *Phil. Trans., Roy. Soc. London*, **A223**, 289 (1923).

Thorson, S. T., "A Study of Calcium Oxalate Dihydrate Crystallization in Synthetic and Human Urines," M.S. Thesis, Univ. Arizona, Tucson (1979).

Manuscript received Oct. 16, 1984, and revision received Oct. 21, 1985.